Analytical and Numerical Investigation of Tube Compression with a Multi-Turn, Axisymmetric Coil

A. Nassiri, S. Zhang, K. Reisert, B. Kinsey*

Department of Mechanical Engineering, University of New Hampshire, USA
*Corresponding author. Email: brad.kinsey@unh.edu

Abstract

While some Finite Element software packages exist that are capable of modelling the electromagnetic forming process and estimating the corresponding process parameters (e.g., magnetic pressure and workpiece velocity), there is a lack of simplified and accuracy analytical modelling tools for this purpose. In this study, a coupled analytical model was created to predict the magnetic pressure generated by a multi-turn, axisymmetric coil and the corresponding tube radial displacement and velocity. In the proposed model, at each time increment, the magnetic field geometry is updated in response to the tube deformation. To assess the proposed analytical model, numerical simulations were conducted where the pressure distribution from the analytical model was applied. The results show good agreement between analytical and numerical results.

Keywords

Forming, Modelling, Electromagnetic tube compression

1 Introduction

The electromagnetic forming (EMF) process is an innovative high speed forming technology widely used in aerospace and automobile industries. It is a safer process than explosive forming and can be easily performed to shape hollow profiles and sheet metal parts made of electrically conductive materials. The setup of EMF includes a fast acting, high power switch; a capacitor bank; a coil; workpiece(s); and additional application specific components, e.g., a mandrel and field shaper for tubular workpieces.

In contrast to the quasi-static forming process, the pressure pulse in EMF causes high strain rate in the workpieces with the entire process being completed O(100μs). The capacitor bank and switch constitute the pulsed power generator. The electrical energy is quickly dissipated into the coil with a damped sinusoidal current trace. A magnetic field is generated, and eddy currents are induced in the workpiece, which flow in the opposite direction to the coil current. These two opposite currents and magnetic fields cause a repulsive Lorentz force between the workpiece and the coil (see Fig. 1). If the Lorentz force is sufficient, the workpiece is plastically deformed or sheared (Nassiri et al., 2014), i.e., if the stress induced is greater than the yield or shear strength of the material, respectively.

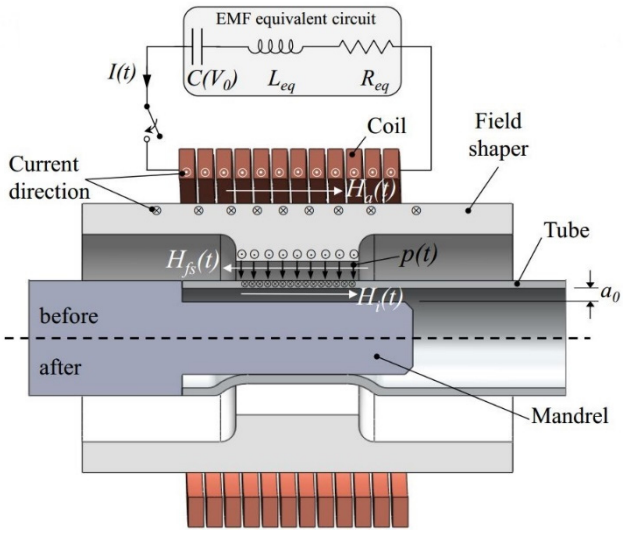

***Figure 1**: Schematic of the Electromagnetic Forming (EMF) process (Geier et al., 2013)*

Numerical simulations of the EMF are beneficial to assess the process as opposed to time consuming and costly experimental investigations. Weddeling et al. (2015) and Lorenz et al. (2014) used two software packages to model the entire EMF process through coupled electromagnetic (ANSYS) and mechanical (LS-DYNA) simulations. Alternatively, Nassiri et al., (2015b) used Abaqus/Explicit for interface investigations during impact welding by simply inputting velocity into the simulations to solve the mechanical component and observed a wavy morphology at the interface. While FEA simulations of the EMF process are effective for estimating the critical process parameters numerically, analytical models can also be effective and less computational and time intensive. Thibaudeau and Kinsey (2015) presented an analytical model to calculate the initial workpiece acceleration, velocity and position during a sheet EMF process with the assumption of rigid body motion of the workpiece. In the analytical model by Hahn et al. (2016), rigid-plastic theory was assumed to represent the material behaviour in response to the forming pressure in magnetic pulsed welding. Finally, similar to the work presented in this paper, Weddeling et al. (2015) numerically and analytically predicted the radial forming displacement during tube compression while also validating the results through experiments.

In this research, an analytical model for determining the pressure distribution applied to the workpiece and the subsequent workpiece radial position and velocity for a multi-turn, axisymmetric coil with field shaper was investigated. In the model, at each time increment, the magnetic field is automatically updated in response to the tube deformation. Compared to previous analytical modelling efforts (Thibaudeau and Kinsey, 2015, Nassiri et al., 2015a, Weddeling et al., 2015, Hahn et al., 2016), a rigid body or a rigid-plastic material assumption was eliminated. Alternatively, plastic deformation of the workpiece during the forming process was taken into account at each time increment. In addition, the coupling factors between the coil, field shaper, and workpiece were experimentally measured and incorporated into the analytical model. The analytical model was then numerically verified using the Abaqus/Explicit to calculate radial position and velocity of the workpiece. Good agreement between the analytical and numerical model results was obtained.

2 Analytical Model

The basic EMF process consists of three fundamental parts: a capacitor bank to store energy, a coil to create the magnetic field, and a workpiece to be formed. Based on the multi-physics nature of the EMF process, the analytical model was divided into three stages. First electrical theory was used to determine the primary current and voltage out of the capacitor bank and passing through the coil. Second, the magnetic field distribution and the effective magnetic pressure that was developed on the workpieces were calculated from electromagnetic analyses. Lastly, classical mechanics theory was used to determine the velocity of the workpiece caused by the effective magnetic pressure. Since the magnetic field distribution strongly depends on the gap distance between the field shaper and workpiece, the magnetic and mechanical processes were coupled. To calculate the workpiece displacement, a simplified plasticity model was incorporated into the algorithm. At each time increment, the magnetics field geometry was updated with an incremental displacement of the workpiece and hence the model includes the new gap between the field shaper and workpiece. See the flowchart of the model in Fig. 2.

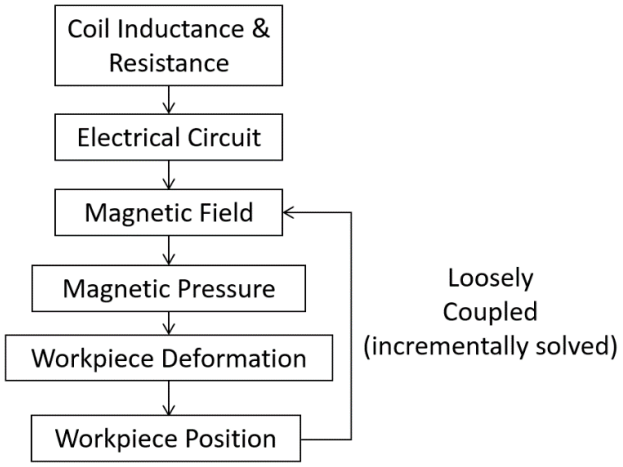

***Figure 2**: Flowchart of the analytical model*

In this study, a commercially purchased multi-turn, axisymmetric coil (Poynting, model: SMU-K100-4/65) was used. The workpiece was a Cu101 tube with a length of 100mm, wall thickness of 0.88mm and outer diameter of 25.36mm. In tube compression processes, usually, a "field shaper" is positioned between the coil and workpiece to concentrate the magnetic field generated (see Fig. 3a and 3b).

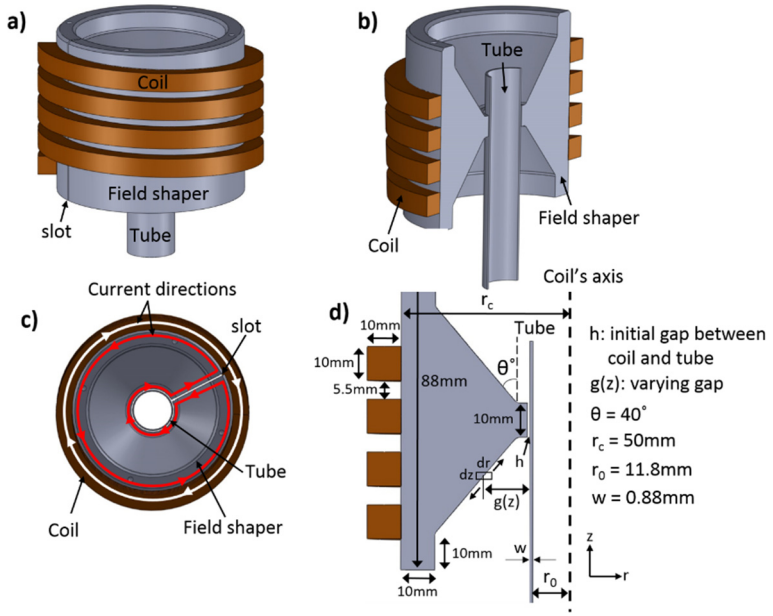

***Figure 3**: Schematic of multi-turn, axisymmetric coil with field shaper and tube: a) full view, b) half view, c) current directions, and d) cross-section*

A quick discharge of the capacitor bank causes a damped sinusoidal current flowing through the coil which induces a related electromagnetic field. Then, in the field shaper which acts as a short circuited second winding of a current transformer, a secondary current is induced. Due to the skin effect and Lenz' law this induced current flows opposite to the coil current at the outer surface of the field shaper (Psyk et al., 2011). At the axial slot, the current is directed to the inner surface of the field shaper in which the current direction is the same as in the coil (see Fig 3c). Compared to the outer surface of the field shaper, the inner area is much smaller, resulting in a higher current density and higher field strength. For this analysis, a series of elements were generated along the surface of the field shaper. The elements were equally spaced, dz, in the axial direction (i.e., z-direction) and the width of each element, dr, was equal to the skin depth (see Fig 3d).

2.1 Electrical Theory

The electrical circuit, consisting of the capacitor bank, coil, field shaper and workpiece, can be represented by ideal electrical elements and circuits (see Fig. 4). As is clear from Fig. 4, both the primary and induced circuits are coupled with the secondary circuit through the mutual inductances (i.e., M_1 and M_2) which are a measure of induction between the two circuits. A "coupling factor" (k) represents the loss of magnetic flux with a value between

$0 \leq k \leq 1$. In this study, the two coupling factors (i.e., k_1 and k_2 corresponding to M_1 and M_2 respectively) were experimentally measured by placing a Rogowski coil in two different locations in the experimental set-up and calculating the ratios of the secondary to primary current ($k_1 = 0.78$) and induced to secondary current ($k_2 = 0.91$). Applying Kirchhoff's voltage law and summing the voltages around the primary circuit, a differential equation is obtained with respect to time, t (Ogata, 2004)

$$\frac{1}{C_m}\int i_p\, dt + i_p R + L\frac{di_p}{dt} = 0 \tag{1}$$

where C_m is the capacitance of the machine, i_p is the current in the primary circuit, $R = R_m + R_c$ is the total resistance, and $L = L_m + L_c$ is the total inductance. Note that the resistance and inductance of the machine, R_m and L_m, can be determined experimentally with a known capacitance by calculating the damped natural frequency and damping ratio of the RLC circuit. Resistance and inductance of the coil, R_c and L_c, are functions of the material properties (i.e., resistivity of the coil), the geometry of the coil, current condition (i.e., the angular frequency), and the cross-sectional area of the coil contained from the skin depth to the surface of the coil. For detailed information see Nassiri et al. (2015a) and Zhang et al., (2004).

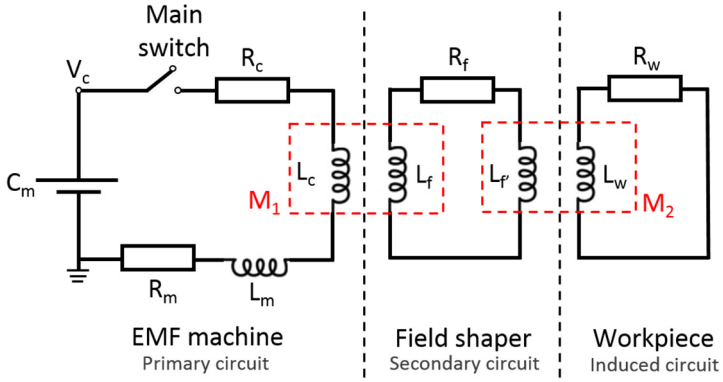

***Figure 4**: Configuration of three circuits and two coupling systems*

To solve the differential equation, i.e., Eq. (1), the initial conditions were specified from the charged capacitor bank with the main switch closing at $t = 0$;

$$i_p(0) = 0, \qquad \frac{di_p}{dt}(0) = \frac{V_i}{L} \tag{2}$$

where V_i is the initial voltage in the capacitor bank

$$V_i = \sqrt{\frac{2E}{C_m}} \tag{3}$$

where E is the total energy stored in the machine. The solution of the differential equation, Eq. (1), yields the variation of the primary circuit current with time and can be expressed as

$$i_p(t) = \frac{V_i}{\sqrt{1-\zeta^2}} \sqrt{C_m/_L}\; e^{-\zeta\omega_n t}\, sin\, \omega_n \sqrt{1-\zeta^2}\, t \tag{4}$$

where ω_n is the natural frequency and ζ is a damping factor of the circuit. Lastly, capacitor voltage can be calculated by integrating the current out of the capacitor

$$V_c(t) = \int -i_p(t)dt \; + \; V_i \tag{5}$$

2.2 Magnetic Theory

The magnetic field produced from a given axisymmetric coil can be determined with respect to the physical location of the tube and the gap distance between the field shaper and tube. As is clear from Fig 2d, because of the tapered geometry of the field shaper, the gap distance is varied along the thickness of the field shaper (i.e., $g(z)$). The magnetic flux density, $\vec{B}$, produced by the coil induces eddy current in the workpiece with a current density, $\vec{J}$. The current density, $\vec{J}$, is related to the magnetic field, $\vec{H}$, through a partial derivative in the radial direction. A Lorentz force is created which acts as a volume force, $\vec{F}$, (Nassiri et al. 2015a)

$$\vec{F} = -\mu_m \vec{H} \frac{\partial \vec{H}}{\partial r} = \; -\frac{1}{2}\mu_m \frac{\partial(\vec{H}^2)}{\partial r} \tag{6}$$

The body force, $\vec{F}$, is integrated through the thickness of the tube to determine the pressure acting on the tube surface

$$\mathrm{P} = \int_0^w \vec{F} dr = \frac{1}{2}\mu_m H_{gap}^2 \tag{7}$$

where the integration limit, w, is the tube thickness (see Fig. 3d) and H_{gap} is the gap magnetic field strength. In this study, the penetrated magnetic field was neglected due to the skin effect. Also, the air space between the coil and workpiece was not considered in the magnetic calculation because its permeability is close to that of free space. The magnetic field strength, H_{gap}, is the resultant field of a superposition of magnetic field strength from many current carrying differential elements, dH_{gap} (see Fig 2d). For the axisymmetric coil investigated in this study, only the magnetic field strength along the coil's axis is of interest (i.e., tangential to the workpiece because this will create a force in the radial direction according to the cross product $\vec{F} = \vec{J} \times \vec{B}$) (Al-Hassani, 1975),

$$H_z = \frac{i}{2\pi}\left[\frac{g(z)-r}{(g(z)-r)^2+z^2} + \frac{g(z)+r}{(g(z)+r)^2+z^2}\right] \quad (8)$$

where $g(z)$ is the varying gap between the coil element and the workpiece and i is the current in the element. As is clear from Eq. (8), the magnetic field strength strongly depends on the radial gap between the field shaper and workpiece.

2.3 Mechanical Theory

Knowing that the workpiece in the forming process is plastically deformed, a simple plasticity model was employed to evaluate the exact deformation of the workpiece in each time increment. Longitudinal and hoop stresses can be easily calculated by knowing the applied external pressure and radius of the workpiece, r, (see Fig 3d).

$$\sigma_L = \frac{Pr}{2w} \;\; \& \;\; \sigma_H = \frac{Pr}{w} \quad (9)$$

The effective stress, assuming von Mises yield criterion was calculated as

$$\bar{\sigma} = \sqrt{{\sigma_H}^2 + {\sigma_L}^2 - \sigma_H\sigma_L} \quad (10)$$

The effective stress, strain and strain-rate relation was defined as

$$\bar{\sigma} = C'\bar{\varepsilon}^n\dot{\varepsilon}^m \quad (11)$$

where C' is the strength coefficient and n and m are the strain and strain-rate hardening exponents respectively. In this study, these parameters were obtained (i.e., $C' = 480\ MPa$, $n = 0.01$, and $m = 0.04$) from Split-Hopkinson Pressure Bar experimental tests on Cu101 (Bragov et al., 2006). The strain rate term in this equation was simply used to shift power hardening curve based on the strain rate in the test. From Eq. (11), $\bar{\varepsilon}$ was calculated. Neglecting the longitudinal strain ($\varepsilon_L = 0$) and considering $d\varepsilon_H + d\varepsilon_t = 0$ (note that this assumption was confirmed experimentally by measuring the axial elongation), the effective strain was evaluated, again assuming von Mises yield criterion, as

$$\bar{\varepsilon} = \frac{2}{\sqrt{3}}\varepsilon_H \quad (12)$$

Finally, the hoop strain, ε_H was calculated from

$$\varepsilon_H = ln\frac{r_{i-1}}{r_i} \quad (13)$$

To obtain the radial location change from time increment, $i-1$, to i, at each axial location. An updated gap between the field shaper and workpiece was then calculated inside a loop by knowing the gap at the previous step and the current incremental displacement of the workpiece. Integrating Eq. (8) over the entire coil thickness yields

$$H_{gap} = \int_0^z \int_0^r H_z dr dy \tag{14}$$

Substituting Eq. (14) in Eq. (7) yields a pressure distribution acting on the workpiece at each time increment. From the radial position data, the velocity of the workpiece was also determined.

3 Numerical Simulations

To validate the analytical result, numerical simulation was performed on the commercial FEA package Abaqus/Explicit. A two dimensional, axisymmetric model was used in this study. The dimensions of the model were exactly the same as mentioned in the analytical modelling section, i.e., length of 100mm, tube thickness of 0.88mm, and outer tube diameter of 12.68mm (see Fig. 5). As in the analytical model, Eq. (11) was also utilized as the material model for Cu101 for the numerical simulations.

For boundary conditions, only the bottom end was fixed in all directions, the top end was free to move. This is consistent with an experimental set-up available for this process. The deformation area was at the middle of the tube where the pressure distribution obtained from analytical model was applied (see Fig. 5). The numerical analysis with the pressure distributions response at both 2.4kJ and 3.6kJ energy discharges were performed. The element type was 4 node, bilinear, axisymmetric, quadrilateral element (CAX4R) with 14400 elements (24 elements through the thickness) in the deformation area (which is 20 mm long based on the pressure distribution) and 1920 elements in the top and bottom areas. A mesh sensitivity analysis was also performed to assure that the mesh density used was not affecting the numerical result.

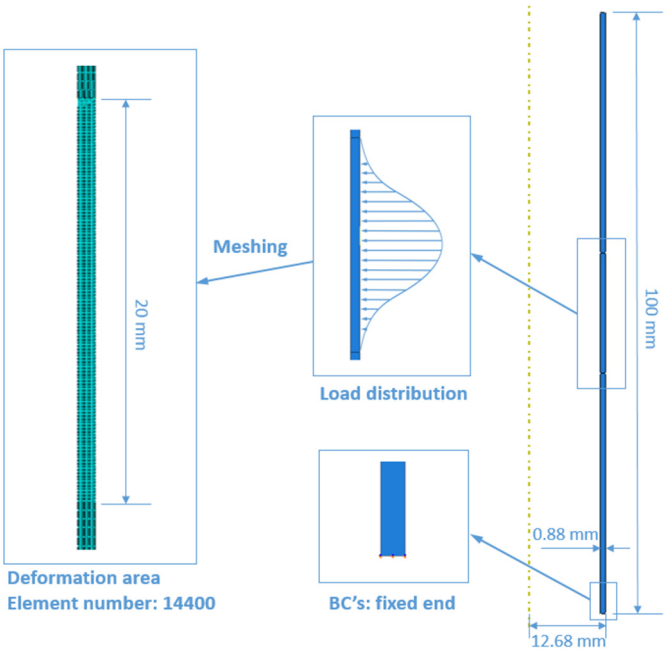

***Figure 5**: Schematic of FEA model*

4 Results

Results from the analytical model include electrical, magnetic, and mechanical predictions. The electrical analysis determines the electrical parameters of the coil and the electrical response of the EMF machine. The predicted circuit response at 2.4kJ energy discharge is shown in Fig. 6 while the spatial magnetic pressure distribution along the workpiece with respect to time is shown in Fig. 7. Clearly for such a coil, the pressure pulse from the first half cycle of the current pulse is more significant than the later oscillations. Thus, the forming event occurs during this timeframe.

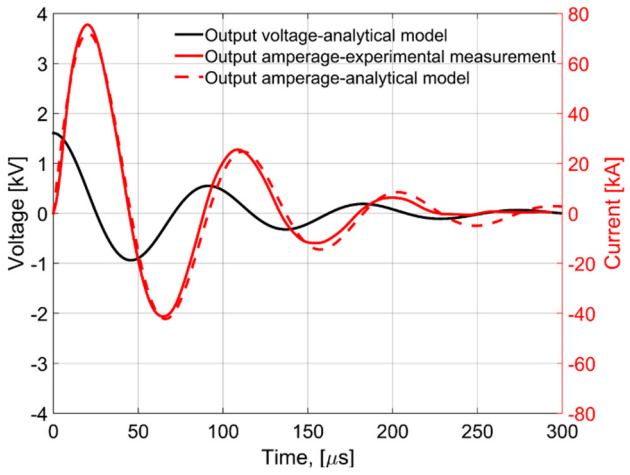

***Figure 6**: Predicted current and voltage during discharge*

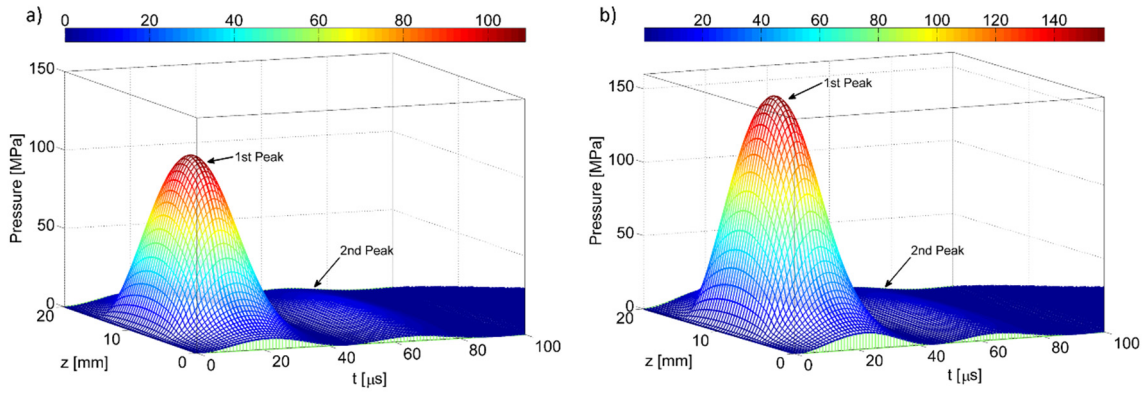

***Figure 7**: Predicted pressure distribution along the tube with time for a) 2.4kJ and b) 3.6kJ cases*

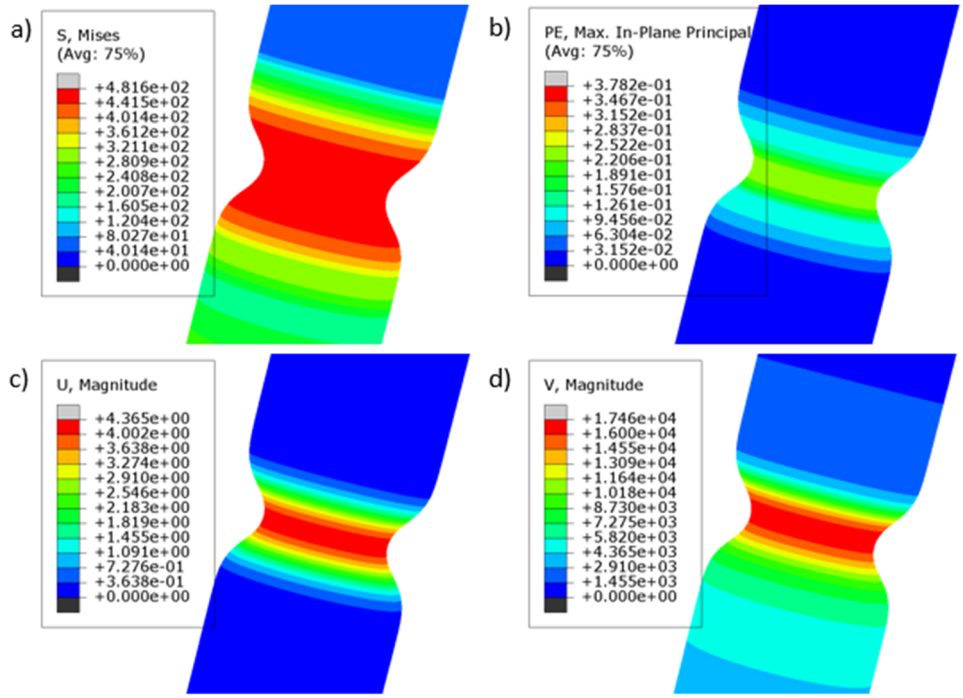

***Figure 8**: FEA results: a) von-Mises stress, b) plastic strain c) radial displacement, and d) radial velocity*

Fig. 8 shows the FEA results for the 3.6kJ energy discharge case with respect to the von-Mises stress, plastic strain, radial displacement, and velocity. Due to the boundary condition that only bottom end was fixed, the results in the axial direction are not perfectly symmetric, e.g., in the non-deformation area. In this case, the axial displacement was only 0.12mm and 0.14mm for 2.4kJ and 3.6kJ energy discharge cases respectively.

Fig. 9 shows the predicted velocity from analytical model and numerical simulations with good agreement demonstrated. The peak velocity from the numerical analyses were 107m/s and 153m/s for 2.4kJ and 3.6kJ energy discharges respectively compared to 106m/s

and 159m/s from the analytical model. The error between these values are 0.9% and 3.9% respectively. The time of the peak velocity is numerically predicted later in the process, but this parameter is less critical for the effectiveness of the process.

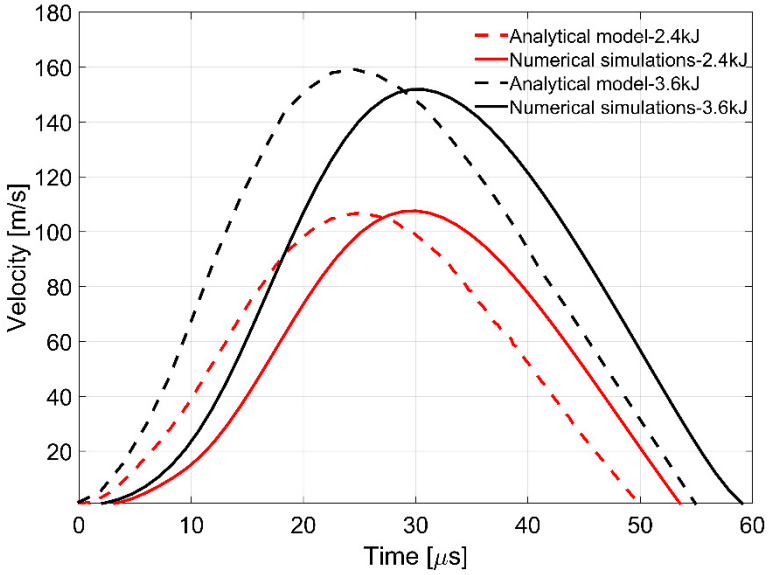

***Figure 9**: Velocity results from the analytical model and numerical simulations*

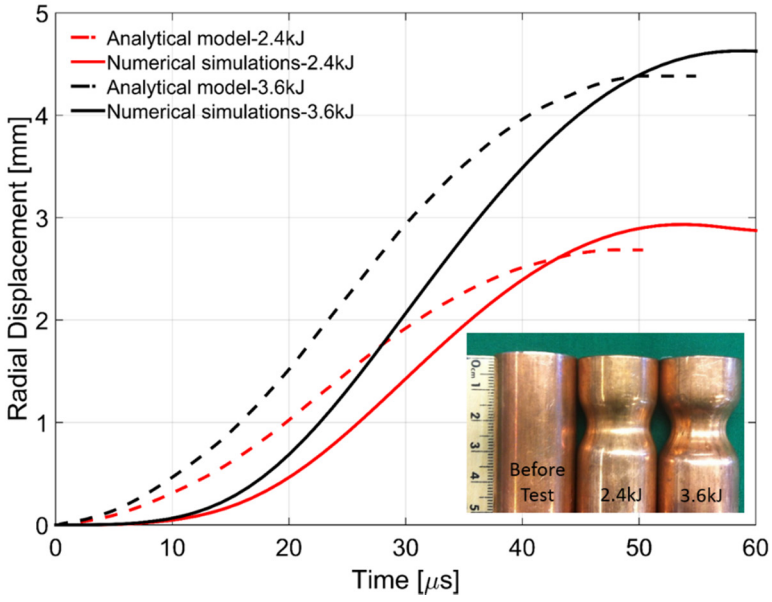

***Figure 10**: Radial displacement from the analytical model and numerical simulations*

The comparison between the predicted radial displacements from the analytical model and numerical analysis is shown in Fig. 10. Again, good agreement is obtained with the peak values being 2.68 mm and 4.38 mm for the analytical model and 2.87 mm and 4.52 mm for the numerical simulations that correspond to 6.6% and 3% differences for the 2.4 kJ and

3.6kJ cases respectively. The data shows that the analytical model approximate the numerical results well. The inset of Fig. 10 includes pictures from experimental tests with Cu101. The slot in the field shaper of the coil (see Fig. 3) causes the process to not be perfectly axisymmetric around the entire perimeter. Also, note that wrinkling is present in the deformed samples.

Some factors used in the modelling efforts were experimentally measured which could account for the discrepancies between the results. For example, the system inductance and resistance were physically measured, but these vary due to resistance heating during the experiments which was not accounted for in the models. The measurement devices and experiment tools may have calibration errors and contribute to the deviations as well. Additionally, the simplification of the material model, used in both modelling efforts, could cause errors. Finally, the analytical model includes various assumptions and simplifications, e.g., the yield criterion and strain assumptions. Therefore, it is difficult to get a precise match between numerical simulations and analytical model results.

5 Conclusions

In this study, an analytical model was set up for the EMF process using a multi-turn, axisymmetric coil and assessed by numerical simulations in Abaqus/Explicit. The results show good agreement between the analytical model and numerical simulations. Compared to the previous analytical modelling efforts, this model incorporates the experimentally determined coupling coefficients in the system and work hardening deformation of the workpiece instead of a rigid body or perfectly plastic material assumption. Therefore, the analytical model is able to predict not only the magnetic pressure distribution on the workpiece, but also the subsequent workpiece velocity and radial displacement. Also, the computational time of the analytical model is considerably less than the FEA simulations.

Acknowledgments

Funding from the U.S. National Science Foundation (CMII-0928319 and CMMI-1537471) is gratefully acknowledged as well as discussions with Yannis Korkolis regarding the analytical model.

References

Al-Hassani, S.T.S., 1975, Magnetic Pressure Distributions in Sheet Metal Forming, Conference on Electrical Methods of Machining, Forming, and Coating, pp. 1–10.

Bragov, A.M., Lomunov, A.K., Abramov, A.V., Konstantinov, A.Y., Sergeichev, I.V., Braithwaite, C., Proud, W.G., Church, P.D., Cullis, I.G. and Gould, P., 2006. The dynamic response of Copper 101 under high-rate loading. In Journal de Physique IV (Proceedings) (Vol. 134, pp. 311-315). EDP sciences.

Geier, M., José, M.M., Rossi, R., Rosa, P.A.R., Martins, P.A.F., 2013. Interference-Fit Joining of Aluminium Tubes by Electromagnetic Forming. Advanced Materials Research 853, pp. 488-493.

Hahn, M., Weddeling, C., Lueg-Althoff, J., Tekkaya, A. E., 2016. Analytical approach for magnetic pulse welding of sheet connections. Journal of Materials Processing Technology, 230, pp. 131-142.

Lorenz, A. Lueg-Althoff J. Goebel, G. Weddeling, C. Beyer, E. Tekkaya, A.E. 2014. Influence of axial workpiece positioning during magnetic pulse welding of aluminum-steel joints. 6th International Conference on High Speed Forming.

Mamalis, A. G., Manolakos, D. E., Kladas, A. G., Koumoutsos, A. K., 2004. Electromagnetic forming and powder processing: Trends and developments. Applied Mechanics Reviews, 57(4), pp. 299-324.

Nassiri, A., Chini, G., Kinsey, B., 2014. Spatial stability analysis of emergent wavy interfacial patterns in magnetic pulsed welding. CIRP Annals-Manufacturing Technology, 63(1), pp. 245-248.

Nassiri, A., Campbell, C., Chini, G., Kinsey, B., 2015a. Analytical Model and Experimental Validation of Single Turn, Axi-symmetric Coil for Electromagnetic Forming and Welding. Procedia Manufacturing, 1, pp. 814-827.

Nassiri, A., Chini, G., Vivek, A., Daehn, G., Kinsey, B., 2015b. Arbitrary Lagrangian–Eulerian finite element simulation and experimental investigation of wavy interfacial morphology during high velocity impact welding. Materials & Design, 88, pp. 345-358.

Ogata, K., 2004. System Dynamics, 4th ed. Pearson Prentice Hall, New Jersey.

Psyk, V., Risch, D., Kinsey, B.L., Tekkaya, A.E., Kleiner, M., 2011. Electromagnetic forming – A review. Journal of Materials Processing Technology 211 (5), pp. 787-829.

Thibaudeau, E., Kinsey, B. L., 2015. Analytical design and experimental validation of uniform pressure actuator for electromagnetic forming and welding. Journal of Materials Processing Technology, 215, pp. 251-263.

Weddeling, C., Demir, O. K., Haupt, P., Tekkaya, A. E., 2015. Analytical methodology for the process design of electromagnetic crimping. Journal of Materials Processing Technology, 222, pp. 163-180.

Zhang, P., Kimchi, M., Shao, H., Gould, J.E., Daehn, G.S., 2004. Analysis of the Electromagnetic Impulse Joining Process a Field Concentrator. AIP Conference Proceeding, pp. 1253-1258.